

University of Arkansas, Fayetteville

ScholarWorks@UARK

Chemical Engineering Undergraduate Honors
Theses


Chemical Engineering

5-2019

Development of a WS₂ Catalyst for Hydrogen Evolution and Improvement via Platinum Nanoparticle Decoration

Alexander O'Brien

Follow this and additional works at: <https://scholarworks.uark.edu/cheguht>

 Part of the [Catalysis and Reaction Engineering Commons](#), and the [Nanoscience and Nanotechnology Commons](#)

Citation

O'Brien, A. (2019). Development of a WS₂ Catalyst for Hydrogen Evolution and Improvement via Platinum Nanoparticle Decoration. *Chemical Engineering Undergraduate Honors Theses* Retrieved from <https://scholarworks.uark.edu/cheguht/140>

This Thesis is brought to you for free and open access by the Chemical Engineering at ScholarWorks@UARK. It has been accepted for inclusion in Chemical Engineering Undergraduate Honors Theses by an authorized administrator of ScholarWorks@UARK. For more information, please contact scholar@uark.edu.

**Development of a WS₂ Catalyst for Hydrogen Evolution
and Improvement via Platinum Nanoparticle
Decoration**

An Honors Thesis submitted in partial fulfillment
of the requirements for Honors Studies in
Chemical Engineering

By

Alexander O'Brien

Spring 2019

Ralph E. Martin Department of Chemical Engineering
College of Engineering
The University of Arkansas

Abstract

In response to a growing global need to improve utilization of green energy, the concept of renewable energy storage via electrolytic hydrogen production has gained popularity in recent years. However, the prohibitive expense of the bulk platinum catalysts currently used for the hydrogen evolution reaction prevents such a concept from being widely adoptable. This research focuses on a possible alternative catalyst, nanolayer WS₂, which is capable of promoting the hydrogen evolution reaction while maintaining economic viability. Bulk WS₂ was prepared in semiconducting, nanolayer form through liquid phase exfoliation. Prepared catalyst inks consisting of this material demonstrated successful hydrogen production. The material was then further improved with the deposition of platinum nanoparticles, forming Pt-WS₂ heterostructures. Optimization of the nanoparticle deposition procedure via the addition of halogen lamp irradiation proved to decrease nanoparticle size, increasing the surface area to mass ratio and augmenting the availability of electron pathways, which resulted in a significant increase in hydrogen production activity. This irradiated Pt-WS₂ sample achieved an onset potential of -62 mV vs RHE and a Tafel slope of 50 mV/decade, placing it among the highest performing transition metal dichalcogenide-based catalysts yet reported.

Acknowledgements

This thesis is the culmination of over three years of work, and I have been aided by a multitude of people that deserve my sincerest thanks for their contributions to my development as a researcher. I'd first like to acknowledge Dr. D. Keith Roper, my chemical engineering advisor, who heard my vague desire to study hydrogen energy as a freshman, guided me to a concrete path of work that needed to be done, and has supported me in that work ever since. I'd also like to thank Dr. Jeremy Dunklin, who began this work with me and taught me the ropes of how to study, think, and solve problems like a scientist while finishing his doctoral work and Ricardo Romo, candidate for MS at the University of Arkansas, who has worked by my side and made unique contributions to this study for the last two years. Lastly, I would like to thank my wife, Kaitlyn, and my parents, Dave and Nancy O'Brien, for their unending support. Thank you to these, and all of the others who have been a part of my undergraduate journey.

Table of Contents

Abstract	1
Acknowledgements	2
1. Introduction	4
1.1 Green energy via hydrogen fuel.....	4
1.2 Catalyst research for hydrogen evolution	5
2. Undecorated WS₂ Catalyst	6
2.1 Preparation of nanoscale WS ₂	6
2.2 Preparation of WS ₂ catalyst inks.....	9
2.3 Electrochemical analysis of WS ₂ catalyst inks	10
2.4 Results and discussion for bare WS ₂ hydrogen evolution.....	13
3. Platinum Nanoparticle Decorated WS₂	16
3.1 Research into TMD material improvements	16
3.2 Platinum reduction onto WS ₂	17
3.3 SEM-EDX and TEM analysis of Pt-WS ₂	19
3.4 Electrochemical analysis of Pt-WS ₂ heterostructures.....	23
3.5 Results and discussion for Pt-WS ₂ catalyst inks	24
4. Conclusion	28
4.1 Summary of methods and results	28
4.2 Recommendations for future work	30
5. References	32

1. Introduction

1.1 Green energy via hydrogen fuel

In response to a growing global need for CO₂ emission-free energy, research into hydrogen (H₂) based fuels has seen a resurgence in popularity in recent years. Hydrogen is an abundant and powerful element, lighter than fossil fuels, yet capable of delivering the energy required to power rockets through a simple reaction that releases only water as a byproduct. [1] Plans have been devised that would allow for hydrogen to be paired with other forms of green, renewable energy as a storage system, which would better enable transport of the electricity gathered from sources such as solar panels or wind turbines, as illustrated in Figure 1. [2] In such plans, energy collected from renewable sources would be used to drive electrolytic water separation and hydrogen ion reduction, a carbon-free process by which hydrogen gas is produced that can be reacted in a fuel cell for electricity as needed, addressing the weather condition based availability issues that currently plague most renewable sources.

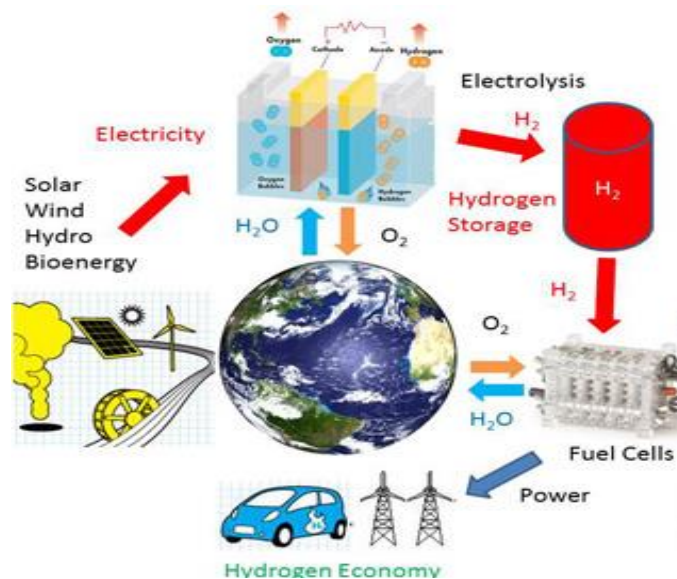


Figure 1: Energy collected from clean, renewable energy sources can be stored as hydrogen fuel via electrolytic separation of water, thus allowing for more efficient utilization of such resources to provide power as needed. [2]

1.2 Catalyst research for hydrogen evolution

Utilization of hydrogen to augment renewable energy is an attractive concept. However, production of H_2 through electrolysis requires significant energy input, necessitating the use of a catalyst to achieve economic feasibility. Bulk platinum/palladium are the most widely used catalysts for this purpose due to their extraordinarily low overpotential requirements for initiation of the hydrogen evolution reaction (HER), [3] [4] [5] but their prohibitive expense and limited availability severely inhibit the widespread growth of the technology. Production of a material with comparable catalytic efficiency but which maintains economic viability for future industrial uses is therefore desirable. Past research centered on addressing this need has focused on a variety of materials, including transition metal carbides, [6] transition metal nitrides, [7] nanoporous graphenes, [8] and graphenes in metal organic frameworks. [9] While these materials may benefit from greater availability and lower associated costs than platinum, their catalytic efficiencies fall well short, and many of them suffer from a lack of industrial scalability.

Considerable recent research has focused on a relatively new form of material, transition metal dichalcogenides (TMDs), which have emerged as promising HER catalysts. [10] [11] [12] [13] TMDs, such as MoS_2 and WS_2 , exhibit unusual optoelectronic characteristics when prepared in nanolayer form, such as low band-gap energy, strong exciton binding, and high electron mobility, all of which are traits which should better enable catalysis of hydrogen ion reduction. The objective of this study has therefore been to determine the catalytic viability of TMDs—specifically WS_2 —for the hydrogen evolution reaction by demonstrating an economically efficient and scalable

method for the production of a WS₂ catalyst, electrochemically testing the capabilities of the produced catalysts, and exploring material improvements which can be achieved through the addition of noble metal nanoparticles to WS₂ nanosheets.

2. Undecorated WS₂ Catalyst

2.1 Preparation of nanoscale WS₂

WS₂, similar to other TMDs, is most commonly available in its bulk form, consisting of multiple nanoscale layers bound together by the attractive van der Waals forces between them, as depicted in Figure 2. [14] In order to optimize the catalytic properties of WS₂, it is necessary to overcome these van der Waals forces and produce 2D-WS₂ in few- to mono-layer form. This separation of layers is commonly accomplished through methods of mechanical cleavage or chemical exfoliation. [15] [16] However, utilization of these processes presents several issues, such as high expense, lack of scalability, and the requirement of toxic or harmful chemicals, which could be expected to impede future growth of the technology to an industrial scale. In this study, materials were prepared at nanoscale via a liquid phase exfoliation process, a method which boasts the advantages of economic efficiency, potential scalability, and a lack of toxic chemical waste, making it a promising prospect for future industrial utilization. [17] Bulk WS₂ (Sigma-Aldrich, St. Louis, MO) was added to a solution of aqueous sodium cholate (C₂₄H₃₉NaO₅, Sigma-Aldrich, St. Louis, MO) and vibrated at high frequency via probe sonication, which provided the energy necessary to shear the van der Waals attracted layers into separate nanolayers. Following sonication, un-sheared materials were

separated from the desired nanolayers via high speed centrifugation and subsequent separation of supernatant and sediment. [18] This process is schematically illustrated in Figure 3.

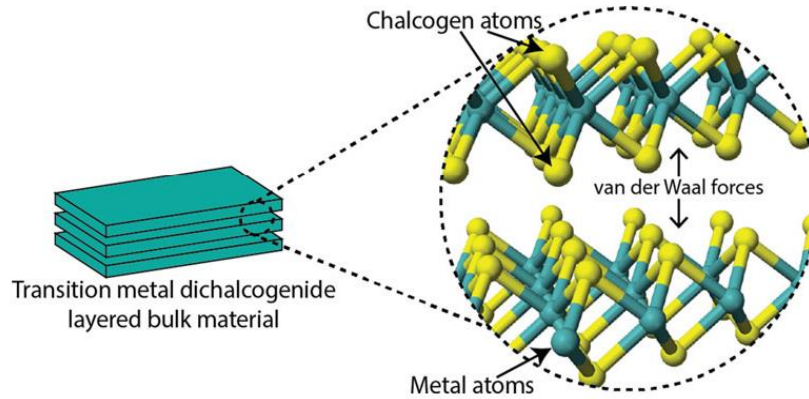


Figure 2: Transition metal dichalcogenides consist of monolayers of metal-chalcogen lattices held together by van der Waals forces. [14]

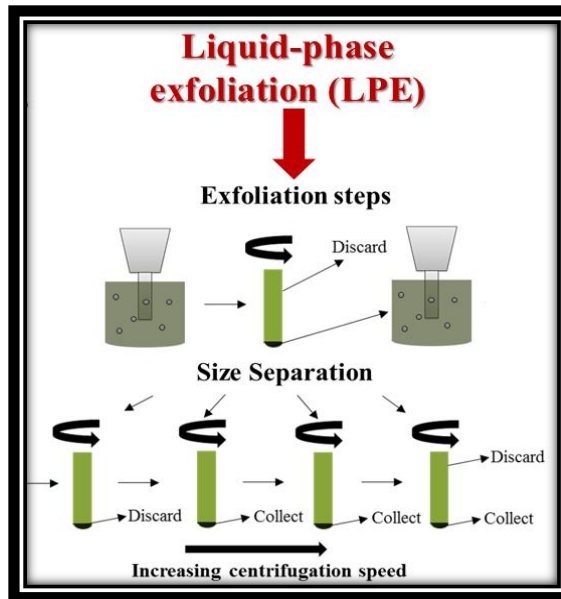


Figure 3: A schematic representation is shown for the liquid-phase exfoliation process of preparing TMDs in nanolayer form. Materials are exfoliated via probe sonication (upper), then size separated via cascade centrifugation (lower). [18]

In addition to the advantages associated with the potential industrial uses of liquid phase exfoliation, the cascade centrifugation portion of the procedure, which follows material sonication, introduces an additional level of material optimization to the process by enabling nanoflake size-selection. By subjecting the sonicated WS₂ to several centrifugation steps at increasing rotational speeds and collecting the acquired sediment at each step, several 2D-WS₂ solutions were prepared with differing average nanoflake sizes. Specifically, the sonicated WS₂ solutions were subjected to four levels of centrifugation at 1000 rpm, 3000 rpm, 4000 rpm, and 6000 rpm. Sediment collected at 1000 rpm was considered to mainly consist of the remaining bulk material or material that had re-aggregated and was accordingly discarded, while the sediments from the following centrifugation steps were preserved. These sediments were each prepared as catalyst inks and electrochemically tested, the procedures for which will be described in upcoming sections. Results of this testing indicated that those nanoflakes which remained in the supernatant following 3000 rpm centrifugation but which fell out as sediment during 4000 rpm centrifugation, herein referred to as 3-4k WS₂, were optimal for catalytic use. The remainder of this work will therefore focus on this 3-4k WS₂ material.

To attain a more in-depth characterization of the 3-4k WS₂ nanoflakes, their dimensions were determined via UV-vis spectroscopy using the following equation:

$$Ext = \epsilon \times C \times L$$

where Ext is the measured extinction, ϵ is the extinction coefficient, C is the nanoflake concentration, and L is the cell length used in spectroscopy. For WS₂, ϵ at 235 nm is known to be relatively invariable at 47.7 L g⁻¹ cm⁻¹. [19] Therefore, this value was

utilized to determine the nanoflake concentrations. Mean nanosheet lengths were then determined by:

$$l(nm) = \frac{2.3 - Ext_{235}/Ext_{290}}{\frac{0.02Ext_{235}}{Ext_{290}} - 0.0185}$$

where l is the mean length. [19] The optimal WS₂ flakes in this study were determined through these equations to have approximately five layers and lateral dimensions of about 100 nm.

2.2 Preparation of WS₂ catalyst inks

To better enable testing of catalytic activity, the exfoliated and size-selected 2D-WS₂ materials were prepared as catalyst inks capable of being drop-cast onto a working electrode. A 1:1 by volume mixture of ethanol and water was added to the extracted nanosheet sediments in order to achieve an approximate concentration of 10 mg/mL WS₂. Figure 4A and 4B display the sediment before and after this dispersal, respectively. To 1.2 mL of this solution, 3 mg of Ketjen superconducting carbon black (EC-600JD, AkzoNobel, Chicago, IL) and 0.3 mL of a 5 mg/mL Nafion ionomer (Sigma-Aldrich, St. Louis, MO) in methanol were added, following the procedure described by Cheng *et al.* [20] These steps resulted in a solution with WS₂ to Ketjen to Nafion mass ratio of 8:2:1, respectively, with the WS₂ concentration being approximately 8 mg/mL. In this solution, the Ketjen black and Nafion materials served to improve conductivity between the glassy carbon working electrode used during testing and the WS₂ nanoflakes, enabling the latter to more effectively utilize applied potential and activate the hydrogen evolution reaction.

Once these materials had been combined, the solution was bath sonicated for 1-1.5 hours to achieve the uniform solution shown in Figure 4C, and the solution was refrigerated at 14°C until electrochemical testing was to be performed.

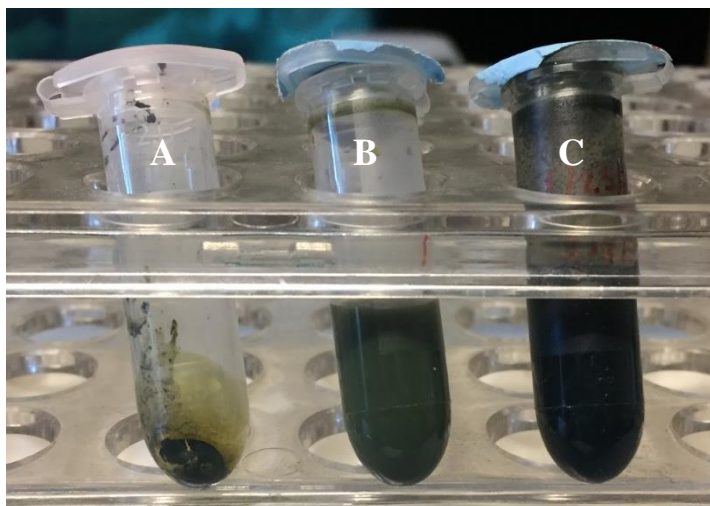


Figure 4: A catalyst ink is shown at different stages of preparation. A) Nanolayer WS₂ has been extracted from the liquid phase exfoliated solution. B) The WS₂ has been dispersed in ethanol and water and displays the dark green color characteristic of WS₂ in its nanolayer form. C) Nafion and Ketjen black have been added to the catalyst solution, and the solution has been bath sonicated to achieve homogeneity prior to electrochemical testing.

2.3 Electrochemical analysis of WS₂ catalyst inks

In general, when a material acts as a catalyst for the hydrogen evolution reaction, it is subjected to an applied potential. This applied potential serves to produce electron-hole pairs, which free up electrons to reduce the attached hydrogen ions from solution and form H₂. With this mechanism in mind, cyclic and linear sweep voltammetry, in which an applied voltage is ramped and the corresponding current is recorded, were determined to be appropriate analyses of a catalyst's efficiency for the hydrogen evolution reaction, as the current measured during testing corresponds to the movement of electrons reducing hydrogen ions in solution.

In order to conduct voltammetric analysis, an electrochemical cell, a schematic of which is shown in Figure 5, was constructed from a three-neck glass flask with a glassy carbon working electrode, a graphite rod counter electrode, and an Ag/AgCl reference electrode in 3 M NaCl. 0.5 M H₂SO₄ was utilized as the electrolyte solution, as it provided an acidic environment with an abundance of H⁺ ions available for reduction without causing rapid corrosion of the electrode materials.

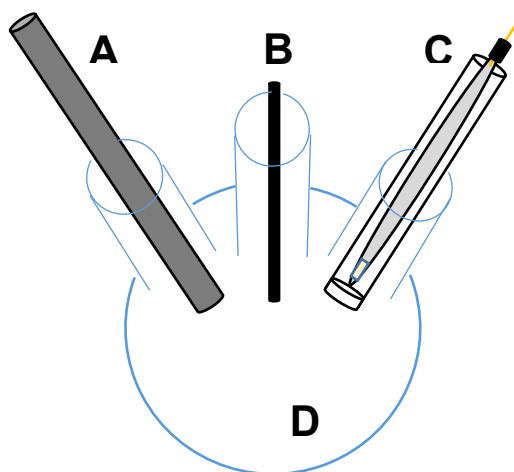


Figure 5: The electrochemical cell set up for performing cyclic and linear sweep voltammetry is shown. The cell consists of A) a graphite rod counter electrode, B) a glassy carbon working electrode, and C) a Ag/AgCl reference electrode in 3M NaCl in D) a glass three-neck flask filled with 0.5M H₂SO₄.

Experiments were performed in this electrochemical cell, which was placed in a fume hood that remained unlit during experiments so that materials were subjected only to ambient light from the lab. The cell was situated on top of a magnetic stir plate, and a stir bar was used within the flask at 900 rpm in order to better enable mass transfer of evolved hydrogen from the tip of the working electrode. Connections were made from the electrodes to a WaveNow potentiostat—purchased, along with the electrodes, from Pine Research Instrumentation, Durham, NC—and lack of contact between the electrodes or between their connections was confirmed visually.

Prior to each test, the working electrode was thoroughly polished to ensure removal of any catalyst material from previous trials. Voltammetry experiments were performed from -200 to -800 mV versus the Ag/AgCl reference electrode. For comparison to reported values in the literature, this voltage was converted to mV versus the reversible hydrogen electrode (RHE) via the following equation:

$$E_{RHE} = E_{Ag/AgCl} + 0.059 \times pH + E_{Ag/AgCl}^{\circ}$$

where E_{RHE} is the voltage versus the reversible hydrogen electrode (V), $E_{Ag/AgCl}$ is the measured voltage with the Ag/AgCl electrode (V), pH refers to the pH value of the electrolyte solution (taken to be 0 for 0.5M H₂SO₄), and $E_{Ag/AgCl}^{\circ}$ is the potential of the Ag/AgCl electrode with respect to the standard hydrogen electrode, which is approximately 0.198 V. During testing, voltage was ramped at a rate of 10 mV/s, and the achieved current was measured. This current was converted to current density (mA/cm²), a more appropriate measure for comparing catalytic efficiency that is not dependent upon electrode size, via the following equation:

$$j = \frac{I}{\pi r^2}$$

where j is the current density (mA/cm²), I is the measured current from the potentiostat (mA), and r is the radius of the cylindrical working electrode (0.15 cm in this work).

For each trial, a background trial was initially performed in which the working electrode was left bare. The prepared catalyst ink was then inverted several times to promote mixing after stationary storage in the refrigerator, and 1.5 μ L of the solution was drop cast onto the tip of the working electrode and allowed to set for 10-15 minutes.

After the setting period, the working electrode was placed back into the electrochemical cell and current was measured across the described voltage range at the described ramp rate. The current measured during background testing, which did not exceed the μA range, was subtracted from the current measured with catalyst in order to determine the current attributable to the catalyst alone. This data was then converted to current density and compared to the voltage versus RHE.

2.4 Results and discussion for bare WS₂ hydrogen evolution

Current density results for the prepared WS₂ inks showed significant increases over the results achieved by the bare working electrode, indicating successful catalysis of the hydrogen evolution reaction. This conclusion was further supported by the visible emergence of hydrogen bubbles on the tip of the working electrode during voltammetry. Additionally, these results were able to be attributed to the WS₂ rather than any other material in the catalyst inks due to control experiments performed involving catalyst inks prepared with identical quantities of water, ethanol, Ketjen, and Nafion to those previously described but without WS₂. These experiments, the results for which are displayed alongside results for an early stage (not optimized for nanoflake size) catalyst ink in Figure 6 below, achieved current densities within the same μA range as the bare electrode, several orders of magnitude below current densities achieved by catalyst inks including WS₂. [21] The direct catalytic activity of the Ketjen black and Nafion materials was therefore determined to be negligible.

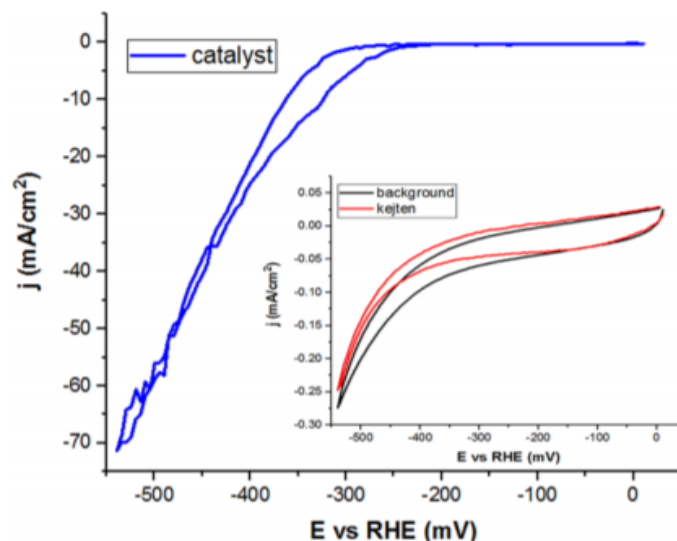


Figure 6: Cyclic voltammetry results provide evidence that materials present in the catalyst ink other than WS_2 play no major role in catalysis of HER. Results are displayed for an early preparation of WS_2 catalyst ink (blue), as well as a catalyst ink prepared identically but without WS_2 (red) and the bare glassy carbon electrode (black). [21]

For those catalyst inks consisting of size-optimized WS_2 nanoflakes, results of voltammetry experiments not only indicated successful catalysis of HER, but also proved competitive with results of several other alternative HER catalysts currently under research [8] [22]. This is indicated by the voltammogram displayed in Figure 7 below, which compares current density results of an 8 mg/mL 3-4k WS_2 with published results for two other HER catalyst alternatives to platinum. This comparison, along with the economic efficiency with which the nanoflake catalyst ink was produced, seems to indicate that WS_2 is a promising alternative material for industrial implementation of HER in the future. However, the achieved current densities still fall substantially short of those achieved by bulk platinum [23], making the widespread adoption of the material unlikely. This difference is chiefly attributed to the high onset potential of WS_2 . The onset potential, described herein as the value of the potential at which voltammetry

achieves a current density of -10 mA/cm^2 , is indicative of the amount of energy that must be input in order to initiate HER, the minimization of which is a primary objective in the development of HER catalysts. For WS_2 and other TMDs, this value is typically around -350 mV , whereas for bulk platinum catalysts the value typically lies around -50 mV or even lower [24]. It is therefore necessary to make further material improvements in order to produce a WS_2 -based catalyst that is catalytically competitive with bulk platinum.

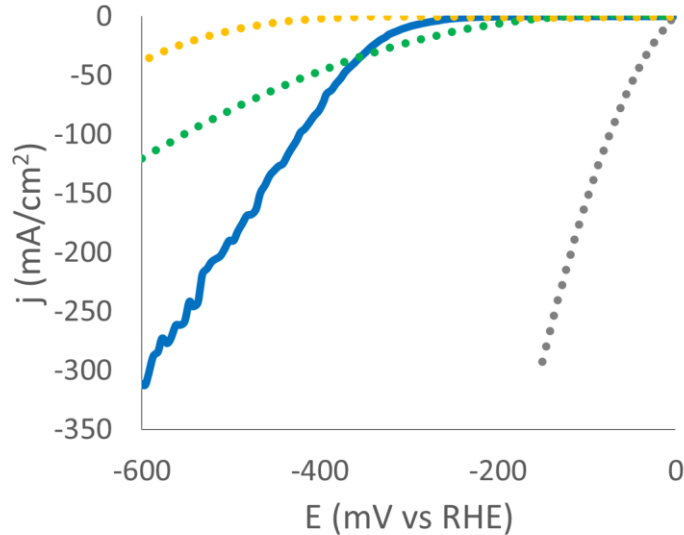


Figure 7: Linear sweep voltammetry data for 8 mg/mL 3-4k WS_2 catalyst ink (blue) is shown alongside reported data for platinum (gray), MoSe_2 (green), and nanoporous graphene (yellow) catalysts. [8] [22] [23]

3. Platinum Nanoparticle Decorated WS₂

3.1 Research into TMD material improvements

Considerable research has been conducted in recent years in order to close the gap in catalytic efficiency between TMD-based HER catalysts and the currently widely implemented bulk platinum catalysts. For instance, TMD nanosheet catalytic efficiency has been demonstrated to increase due to association with electroactive substrates like oxidized carbon fiber and graphite foam. [25] [26] In other cases, enhancements have been achieved through modification of the TMD phase by chemical exfoliation preparation techniques to achieve increased concentration of metastable metallic 1T-phase nanoflakes, as opposed to the more common semiconducting 2H-phase, thereby increasing the number of defect sites at which hydrogen ion reduction can occur. [11] [27] Augmentation of HER activity has also been achieved by the attachment of metal co-catalysts such as iron, cobalt, nickel, and gold onto TMD nanosheets. [28] [29] [30]

Based on the results of these metal co-catalyst experiments, it was hypothesized that the utilization of platinum nanoparticle co-catalysts could enable significant catalytic improvements in the bare WS₂ materials described in previous sections of this work. Such heterostructures were expected to achieve the extremely low onset potentials characteristic of platinum catalysts while still minimizing use of the noble metal and maintaining cost effectiveness. These results have been previously demonstrated by Huang *et al.*, who achieved the epitaxial growth of Pt-nanostructures on lithium-intercalated 1T-MoS₂ nanosheets, [27] as well as by Zhang *et al.*, who followed a procedure similar to that of Huang to deposit PtNPs onto hydrothermally prepared WS₂ nanosheets. [31] In both cases, catalytic performance was significantly improved over

that of the undecorated TMD material. However, prior to the work by our group described herein, [32] no data had yet been reported for Pt deposition onto 2H-phase WS₂ nanosheets obtained by liquid phase exfoliation, a material which benefits from a production method with the potential for future industrial growth while also maintaining the unique optoelectronic properties of the 2H-phase, which may enable further light induced improvements in the future. [33] [34] Furthermore, the effects of light irradiation on PtNP deposition and the subsequent changes in catalytic activity had not yet been explored. In order to meet this need, a procedure was adapted from that described by Huang *et al.* [27] to deposit PtNPs onto WS₂ nanoflakes prepared via the methods described in the preceding sections.

3.2 Platinum reduction onto WS₂

For this deposition, a 3.9 mg/mL solution of 3-4k WS₂ nanoflakes in water was prepared. 18 mg of potassium tetrachloroplatinate (II) (K₂PtCl₄) powder (Sigma-Aldrich, St. Louis, MO) and 20 mg of sodium citrate tribasic dihydrate (C₆H₅Na₃O₇·2H₂O) powder (Sigma-Aldrich, St. Louis, MO) were combined in a crystal cuvette, and deionized water was added to reach a volume of 3 mL. In this solution, K₂PtCl₄ served as a source for the necessary Pt ions, and citrate was added to act as a reducing and stabilizing agent for the PtNPs, as has been previously demonstrated with graphene [35] [36] [37] and TMDs [27] [31]. To this mixture, 167 μL of the prepared WS₂ solution was added while the mixture was stirred at 900 rpm with a magnetic stir bar. This resulted in a WS₂-substrate catalyzed deposition bath in which the Pt ions were reduced and deposited onto the surface of the WS₂ nanoflakes, similar to methods of electroless deposition

commonly used for microelectronics and polymer substrates. [38] [39] [40] This process is schematically represented in Figure 8 below. Two reaction solutions were produced via this method simultaneously, and, following the introduction of the WS₂ material and the subsequent initiation of the chemical reduction and deposition of Pt ions, these solutions were allowed to react for two hours. In order to analyze the effects of light irradiation on this Pt deposition procedure, one of these solutions was placed in a fume hood directly under a 150 W halogen lamp for the duration of the two hours, while the other was placed in an unlit fume hood and subjected only to ambient light from the lab. The resultant Pt-WS₂ heterostructures will be referred to in the remainder of this report as Pt-WS₂(L) and Pt-WS₂(NL) for the materials produced in the presence and absence of the halogen lamp, respectively. The cuvettes in both cases were kept in ice baths that were frequently resupplied to maintain both solutions at similar temperatures so that the only difference in production procedures was the presence of irradiation from the halogen lamp. After two hours of reaction time, unreacted and aggregated materials were separated from the desired Pt-WS₂ heterostructures via high speed centrifugation. The WS₂ nanoflakes decorated with PtNPs were then ready for subsequent characterization and electrochemical testing.

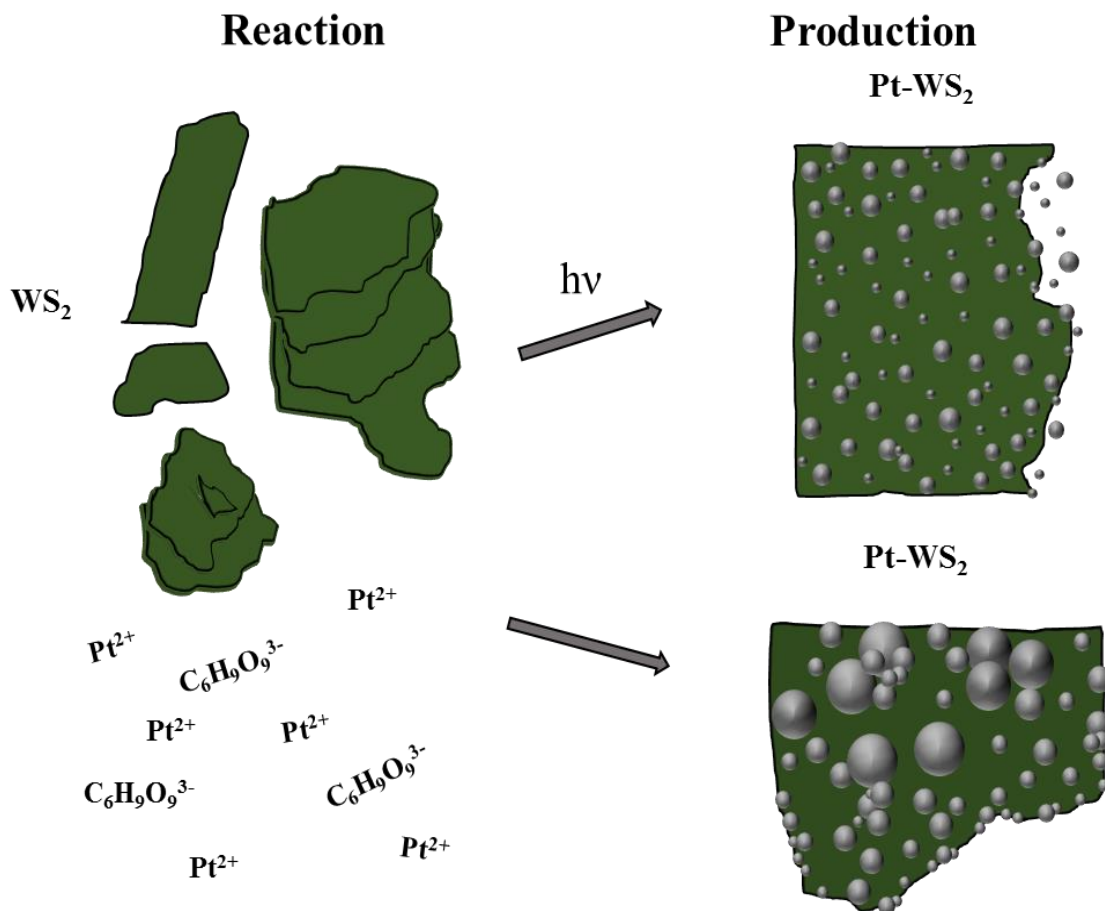


Figure 8: Schematic representation of light-modulated electrochemical PtNP deposition on WS_2 nanosheets. An aqueous sodium cholate suspension of liquid exfoliated WS_2 nanosheets (upper left) was mixed with potassium tetrachloroplatinate (K_2PtCl_4) and sodium citrate tribasic dihydrate ($C_6H_5Na_3O_7 \cdot 2H_2O$). Upper right shows $Pt-WS_2$ adduct consisting of 36 nm x 50 nm WS_2 nanosheet with 1-3 nm PtNPs uniformly dispersed.

This adduct was generated with a 150 W halogen lamp. Lower right shows $Pt-WS_2$ adduct consisting of 33.75 nm x 27.5 nm WS_2 nanosheet with 1-5 nm PtNPs and larger aggregates. This adduct was generated at ambient light conditions with no halogen lamp.

[32]

3.3 SEM-EDX and TEM analysis of $Pt-WS_2$

Newly produced $PtNP-WS_2$ nanosheet heterostructures were subjected to energy-dispersive x-ray via scanning electron microscope (SEM-EDX) as well as transmission

electron microscopy (TEM) imaging at the University of Arkansas Nano-Bio Materials Characterization Facility to provide detailed descriptions of the distribution and size composition of deposited PtNPs. SEM-EDX spectroscopic analysis, performed using an FEI Quanta 200 instrument operating at 30.0 kV, confirmed the uniform presence of atomic platinum (Figure 9B) among the detected tungsten (Figure 9C) and sulfur (Figure 9D) elements of the nanoflakes. This confirmation is key to the proceeding experiments, as it verified the effectiveness of the described PtNP deposition procedure, allowing for differences in results for electrochemical testing of Pt-WS₂ compared to undecorated WS₂ to be rightfully attributed to the addition of PtNPs. SEM-EDX analysis also allowed for the determination that PtNP deposition occurred along both the basal and edge planes of the WS₂ flakes. This contrasts results achieved by the spontaneous reduction of gold nanoparticles onto WS₂ flakes from a gold (III) chloride solution, which was reported to produce gold nanoparticles (AuNPs) preferentially on uncoordinated edge sulfurs of WS₂ by means of an Au-S covalent bond. [33] Nanoparticle decoration across the entirety of the WS₂ nanoflakes, as opposed to solely along the edge sites, results in drastically higher nanoparticle surface area availability, indicating that the PtNP decorated materials should be more conductively enabled than the AuNP decorated materials. It also suggests that an additional mechanism for bonding is present beyond the covalent bonding to edge sulfurs seen with AuNPs, which is to be expected to some degree since PtNPs were deposited in the presence of a reducing agent, citrate.

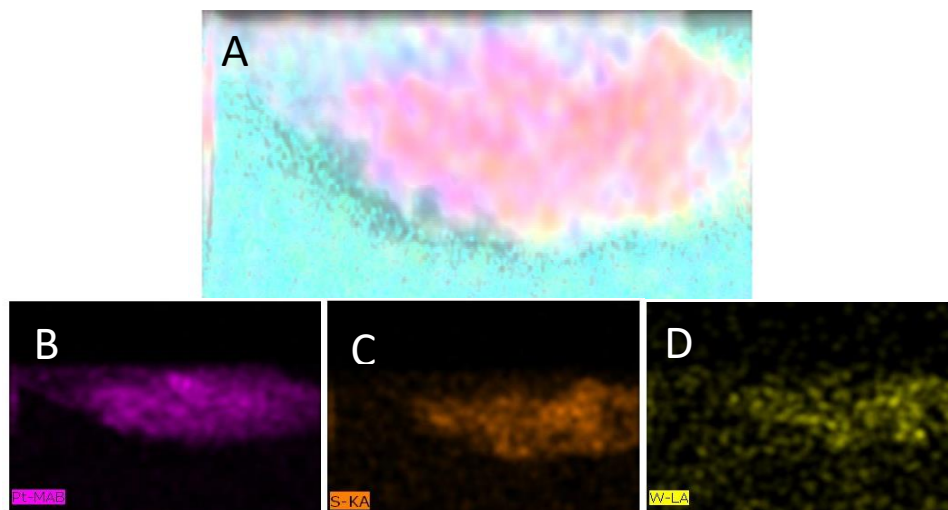


Figure 9: SEM-EDX imaging allowed for confirmation of WS₂ nanoflake decoration with PtNPs and provided information regarding the extent of deposition. A) Comprehensive SEM-EDX elemental mapping is shown for Pt-WS₂(L) (pink/yellow/orange) on 20 nm thick SiO₂ TEM grid membrane (teal). Specific elemental mapping is also shown for B) platinum, C) sulfur, and D) tungsten. [32]

Following determination of the presence of PtNPs through SEM-EDX analysis, TEM imaging allowed for more in-depth analysis into the size and distribution of deposited PtNPs. Comparison of Pt-WS₂(L) and Pt-WS₂(NL) through this method revealed significant differences in nanoparticle morphology. TEM images for Pt-WS₂(L), displayed in Figure 10A, revealed homogenous distribution of nanoparticles across the WS₂ nanoflake surface with near uniform size distribution. The mean average diameter for these PtNPs, taken from a sample size of fifteen nanoparticles, was calculated to be 2.05 nm. [32] By comparison, images taken for Pt-WS₂(NL), displayed in Figure 10B, revealed notably more irregular distribution of PtNPs. A sample size of fifteen nanoparticles for this material resulted in a mean average diameter of 3.84 nm, nearly

two-fold higher than that of Pt-WS₂(L), and a small proportion of PtNPs were found to have diameters upwards of 7 nm. [32]

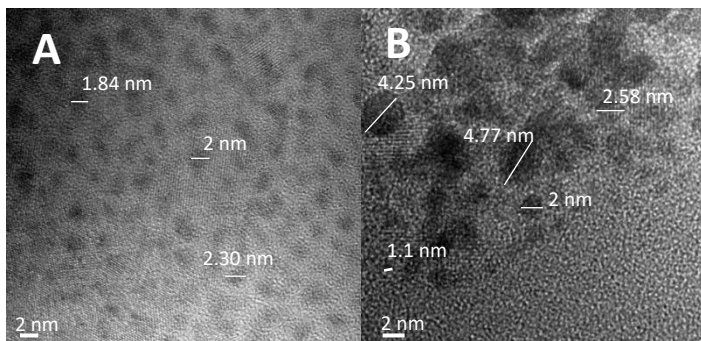


Figure 10: Transmission electron microscopy (TEM) images for Pt-WS₂ samples indicate that the use of the halogen lamp during reduction leads to smaller, more uniform PtNP decoration. Images are shown for A) Pt-WS₂(L) and B) Pt-WS₂(NL). Individual PtNPs on the WS₂ material have been sized and labeled for each image. [32]

The described variation in size and homogeneity of nanoparticles between the Pt-WS₂(L) and Pt-WS₂(NL) materials is expected to be due to a change in reduction mechanism caused by the presence of irradiation from the halogen lamp. In the absence of light or in ambient light from the lab, PtNP deposition proceeds primarily through redox reaction, whereby the Pt(II) ions present in solution from the K₂PtCl₄ material dispersion are reduced to Pt(0) and are capable of depositing directly on the WS₂ nanoflake surfaces or aggregating with adjacent PtNP deposits to form larger clusters. [41] With the addition of light from the halogen lamp, redox reaction is more significantly complemented by the presence of a photoelectric effect from the WS₂ nanoflakes. [42] In this case, high absorption of photons from the WS₂ causes the formation of electron-hole pairs. Long-lived excitons from this effect better enable the

direct reduction of Pt ions onto WS₂ nanosheet surfaces, causing a preferential pathway of reduction that results in the formation of more nanoparticles and inhibits aggregation, limiting nanoparticle size. This explanation is consistent with the results of the performed TEM analysis, and it suggests a method of control and optimization for nanoparticle deposition on TMDs that could merit more detailed exploration in the future. Further research into such light-tuned deposition is expected to be especially valuable for 2H-WS₂, which has unique optoelectronic properties that could enable more precise utilization of light at specific wavelengths.

3.4 Electrochemical analysis of Pt-WS₂ heterostructures

Following two hours of reaction time, the K₂PtCl₄, citrate, and WS₂ solutions were subjected to high speed centrifugation, and the desired Pt-WS₂(L) and Pt-WS₂(NL) adducts were extracted as the sediment. These sediments were then prepared as catalyst inks following the same method described for undecorated WS₂, in which the sediment was combined with ethanol, water, Nafion ionomer, and Ketjen black and bath sonicated for 1-1.5 hours to achieve homogenous solutions. Voltammetric testing was then conducted to determine the catalytic capabilities of these materials. As previously described, a three-electrode system using a glassy carbon working electrode, graphite rod counter electrode, and Ag/AgCl reference electrode with 0.5 M H₂SO₄ electrolyte was utilized in conjunction with a WaveNow potentiostat to collect current density data. All trials were conducted from -200 to -800 mV versus the Ag/AgCl electrode at a rate of 10 mV/s in an unlit fume hood and with a magnetic stir bar at 900 rpm. Trials were first conducted for the bare electrode as a background measure. Trials were then conducted for

the Pt-WS₂(NL) ink, the Pt-WS₂(L) ink, and an undecorated WS₂ ink prepared from the same sample of WS₂ utilized for the platinum decorated material and at approximately the same concentration. This combination of data allowed for the direct comparison of HER catalytic improvement achieved for a WS₂ sample upon decoration with PtNPs and the effect upon catalytic activity of nanoparticle size, as measured with TEM imaging. The glassy carbon working electrode was polished between each trial to completely remove material from previous tests. In each case, the desired catalyst was inverted several times to ensure good mixing and 1.5 μL was drop-cast onto the tip of the polished working electrode and allowed to set for 10-15 minutes.

3.5 Results and discussion for Pt-WS₂ catalyst inks

Linear sweep voltammetry results for the Pt-WS₂(NL), Pt-WS₂(L), and undecorated WS₂ catalyst inks are shown in Figure 11A below. At peak tested voltage, Pt-WS₂(NL) catalyst achieved current density 1.3 times greater than that obtained by the undecorated WS₂, while Pt-WS₂(L) achieved current density 2.5 times greater. These results indicate that the presence of PtNPs increases catalytic activity over undecorated WS₂, as hypothesized. Results also indicate that the effect of these PtNPs was significantly increased for smaller, more uniformly distributed PtNPs, as opposed to large clusters. This was to be expected, as the large quantity of smaller nanoparticles results in a significantly increased surface area to mass ratio for the PtNPs, augmenting the surface area available for proton reduction and increasing the quantity of accessible electron pathways. Additionally, these results are consistent with the results presented by Tan *et al.*, who suggested that an optimal HER activity per unit mass of PtNPs absent TMDs

occurs at nanoparticle diameters of approximately 2.2 nm, with specific mass activity decreasing for particles above or below this point. [43] The mean average diameter of 2.05 nm measured for PtNPs present in the Pt-WS₂(L) heterostructure falls very close to this stated optimal point, differing by less than 0.2 nm. On the other hand, with the mean average diameter of 3.84 nm and the overall lack of uniformity in nanoparticle size, few nanoparticles present on the Pt-WS₂(NL) surface approach this optimized size of 2.2 nm as closely as those present in Pt-WS₂(L), suggesting that catalytic effectiveness would be expected to be greater for those particles prepared under halogen lamp.

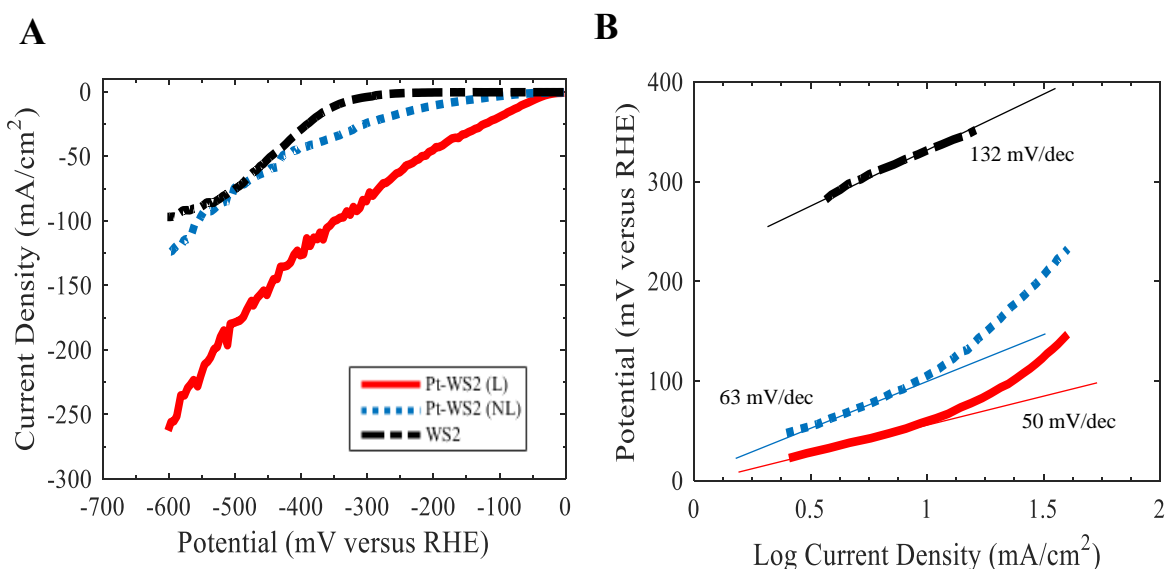


Figure 11: A) Linear sweep voltammetry results and B) Tafel slope results for Pt-WS₂(L) and Pt-WS₂(NL) alongside results for a sample of Pt-free WS₂. [32]

Although these results for current density at peak voltage seem to indicate the apparent catalytic superiority of the Pt-WS₂(L) compared to the Pt-WS₂(NL) and undecorated WS₂ materials, data at peak voltage is somewhat imprecise for comparison to other literature reported data, as the high levels of mass transfer associated with hydrogen gas production at the tip of the electrode cause interference with measured

current. This is evident in Figure 11A, in which the linear sweep data becomes significantly more erratic at high levels of voltage and high current densities, when hydrogen production is at its peak. For more careful comparisons therefore, voltammetric data was also analyzed in terms of onset potentials and Tafel slopes.

Onset potential is defined in this work similar to previously published reports as the applied potential required for a catalyst to achieve a current density of -10 mA/cm^2 during linear sweep voltammetry. This value is indicative of the energy input required to achieve a significant rate of reaction, with a near-zero value indicating that very little energy is required to initiate the production of hydrogen gas. Minimization of the onset potential is therefore a primary objective in the development of HER catalysts, as lower required energy input allows for increased efficiency and decreased cost associated with production. For the undecorated WS_2 obtained by liquid phase exfoliation, which was considered in Figure 11 of this report, an onset potential of -350 mV vs RHE was recorded, a typical value for a bare TMD nanosheet. The addition of PtNPs in the absence of light, i.e. Pt- $\text{WS}_2(\text{NL})$, reduced this onset potential significantly to -195 mV vs RHE , while the smaller PtNPs obtained with the halogen lamp in the Pt- $\text{WS}_2(\text{L})$ sample further reduced the value to -62 mV vs RHE . [32]

Data was also collected regarding the Tafel slopes of each material, which relates the kinetics of the chemical reaction at the electrode to the applied overpotential. This is a preferred method of analysis in some reports, as the Tafel slope is roughly constant for a material with respect to mass per unit area, whereas the onset potential can often be decreased with increasing mass of deposited TMD per unit area on the electrode. [44] Tafel slope is calculated as the slope of the overpotential, η , versus the natural log of

current density, i , relative to exchange current density, i_0 . This slope often exhibits increased values at higher overpotentials, but the accepted values are those taken where the plots of η versus $\ln(i/i_0)$ are linear, where the current density is typically proportional to polarization. [45] Like onset potential, a near-zero Tafel slope is desirable for an HER catalyst, as this indicates that a high increase in current density can be achieved with very little increase in applied voltage. As displayed in Figure 11B, the undecorated WS₂ achieved a relatively high Tafel slope of 130 mV/decade, which the Pt-WS₂(NL) material approximately halved with 63 mV/decade and which the Pt-WS₂(L) further improved upon with 50 mV/decade. [32]

As can be viewed in Figure 12, the reported values for the discussed undecorated WS₂ place it on the low end of the spectrum for catalyst performance, falling well short of all decorated TMD materials and even underperforming some other undecorated WS₂ materials. However, this same material used in the Pt-WS₂(L) heterostructure achieves highly competitive catalytic results comparable to that of the 1T Pt-MoS₂ produced by Huang *et al.* and surpassing currently reported data for all other WS₂-based catalysts, including the Pt-WS₂ produced by Zhang *et al.* [27] [31] This material is considerably surpassed only by reduced graphene oxide decorated with a combination of platinum and palladium, which may suggest that this noble metal combination should be considered with WS₂ for further improvement in the future.

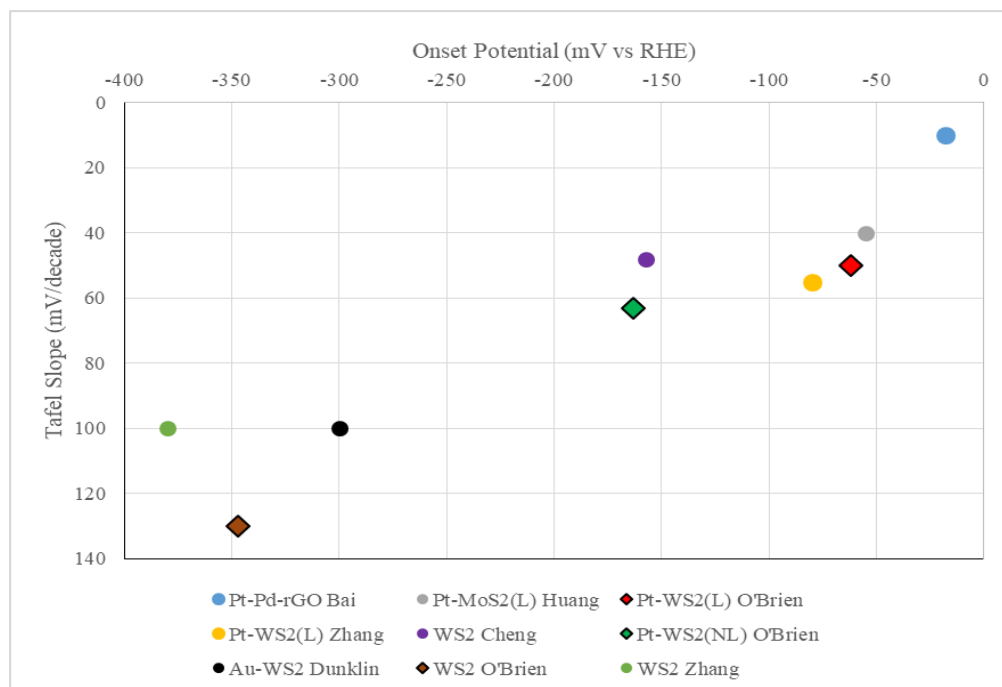


Figure 12: Onset potential versus Tafel slope data shown for various reported HER catalysts indicates that the Pt-WS₂(L) discussed in this report is among the highest performing catalysts and is the highest performing WS₂-based catalyst, whereas an undecorated WS₂ catalyst prepared from the same material is among the lowest. Data displayed as diamonds represent materials examined in this report. Minimization of both Tafel slope and onset potential (upper-right portion of the graph) are the desired traits for a successful catalyst. [20] [27] [31] [32] [33] [46]

4. Conclusion

4.1 Summary of methods and results

Hydrogen gas, a carbon-free energy source, can be produced via electrolysis with electricity from renewable energy sources such as solar and wind, enabling improved portability and storage of energy from such sources. Research discussed in this report was intended to improve the economic feasibility of hydrogen evolution via electrolysis by utilizing the unusual optoelectronic properties achieved in transition metal dichalcogenides by preparation in few- to mono-layer nanosheets. Undecorated WS₂

nanoflakes were prepared in the semiconducting 2H-phase through liquid phase exfoliation, an inexpensive and scalable method. Prepared nanoflakes were size-selected by cascade centrifugation, and optimal nanoflakes for catalysis were determined to be those collected as sediment between 3000 and 4000 rpm centrifugations with average layer numbers of 5 and average lateral dimensions of approximately 100 nm. Select samples of these 3-4k WS₂ nanoflakes were decorated with PtNPs via chemical reduction with K₂PtCl₄ and citrate under halogen lamp irradiation. Other samples were decorated via chemical reduction while subject only to ambient light conditions from the lab, and still more samples were left undecorated.

Prepared WS₂, Pt-WS₂(NL), and Pt-WS₂(L) samples were prepared into catalyst inks by combination and sonication with Nafion ionomer, Ketjen superconducting carbon black, ethanol, and water. Catalytic activities of these inks were electrochemically tested via linear sweep and cyclic voltammetry experiments in a three-electrode cell with a 0.5 M H₂SO₄ electrolyte. Results for undecorated WS₂ confirmed the hydrogen production capabilities of the material and proved competitive with certain other alternative HER catalyst materials but fell well short of the top performing materials. Results for Pt-WS₂(NL) improved onset potential compared to the undecorated material from -350 mV vs RHE to -160 mV vs RHE and Tafel slope from 130 mV/decade to 63 mV/decade. [32] Results for Pt-WS₂(L) then achieved further improvement with an onset potential of approximately -62 mV vs RHE and Tafel slope of 50 mV/decade. [32] Both of these results were among the lowest yet reported for semiconducting nanosheet based catalysts, and the onset potential result was the lowest yet reported for a WS₂-based catalyst.

PtNPs present in the Pt-WS₂(NL) and Pt-WS₂(L) heterostructures were compared via TEM imaging. PtNPs in the Pt-WS₂(L) structure were found to be smaller and more uniformly dispersed. Average nanoparticle diameter of these nanoparticles was calculated to be 2.05 nm, while the average diameter for Pt-WS₂(NL) PtNPs was calculated at 3.84 nm. Differences in catalytic performance were attributed to these observed differences in nanoparticle sizes. Smaller PtNPs present in the Pt-WS₂(L) heterostructures increased surface area available for proton reduction, thereby augmenting electron transport and achieving reduced onset potentials and Tafel slopes.

4.2 Recommendations for future work

Based on the results of Pt-WS₂(L) in the achieved work, WS₂-based catalysts produced via liquid phase exfoliation may be expected to serve as useful catalysts for hydrogen production at the industrial scale in the future, and further research into material improvements is strongly recommended. As previously mentioned, such research could be focused on adjustments to the noble metal nanoparticle co-catalysts, such as forming combined platinum/palladium nanoparticles. Further optimization is also likely achievable in terms of the platinum-only nanoparticles with further tuning of nanoparticle sizes and distributions. The amount of K₂PtCl₄ and citrate utilized in decoration could almost certainly be decreased with respect to the amount of WS₂, subsequently decreasing associated costs of production and minimizing waste.

Possibly the largest area in which potential improvements are expected to be achieved in the future is in the use of light sources to utilize the optoelectronic properties

inherent to the 2H-phase of WS₂. Decreased size in nanoparticles under halogen light irradiation was attributed to a photoelectric effect in the WS₂ increasing the presence of electron-hole pairs. Such an effect could likely be utilized during production of hydrogen as well, and more precise control of the wavelength and power of light to which the catalyst was subjected during hydrogen production would likely allow for more optimized control of production.

References

- [1] M. Boyles and V. Dawson, Taming liquid hydrogen: The centaur upper stage rocket, Washington, DC: National Aeronautics and Space Administration Office of External Relations, 2004.
- [2] J. Wang, "Barriers of scaling-up fuel cells: Cost, durability and reliability," *Energy*, vol. 80, pp. 509-521, 2015.
- [3] A. Alaswad, A. Baroutaji, H. Achour, J. Carton, A. A. Makky and A. G. Olabi, "Developments in fuel cell technologies in the transport sector," *Int. J. Hydrogen Energy*, vol. 41, no. 37, pp. 16499-16508, 2016.
- [4] F. Barbir, "PEM Fuel Cells," in *Sammes N. (eds) Fuel Cell Technology*, London, Springer, 2006, pp. 27-51.
- [5] N. Cheng, S. Stambula, D. Wang, M. N. Banis, J. Liu, A. Riese, B. Xiao, R. Li, T. Sham, L. Liu, G. A. Botton and X. Sun, "Platinum single-atom and cluster catalysis of the hydrogen evolution reaction," *Nature Communications*, vol. 7, p. 13638, 2016.
- [6] Y. Regmi, G. Waetzig, K. Duffee, S. Schmuecker, J. Thode and B. Leonard, "Carbides of group IVA, VA and VIA transition metals as alternative HER and ORR catalysts and support materials," *Journ. Mat. Chem. A*, vol. 3, no. 18, pp. 10085-10091, 2015.
- [7] Y. Li, J. Zhang, X. Qian, Y. Zhang, Y. Wang, R. Hu, C. Yao and J. Zhu, "Nanoporous niobium nitride (Nb₂N) with enhanced electrocatalytic performance for hydrogen evolution," *Applied Surface Science*, vol. 427, pp. 884-889, 2018.
- [8] A. Eftekhari, "Electrocatalysts for hydrogen evolution reaction," *Inter. J. of Hydrog. Ener.*, vol. 42, no. 16, pp. 11053-11077, 2017.
- [9] M. Jahan, Z. Liu and K. Loh, "A graphene oxide and copper-centered metal organic framework composite as a tri-functional catalyst for HER, OER, and ORR," *Advanced Functional Materials*, vol. 23, no. 43, pp. 5363-5372, 2013.
- [10] T. Jaramillo, K. Jorgensen, J. Bonde, J. Nielsen, S. Horch and I. Chorkendorff, "Identification of active edge sites for electrochemical H₂ evolution from MoS₂ nanocatalysts," *Science*, vol. 317, no. 5834, pp. 100-102, 2007.
- [11] D. Voiry, M. Salehi, R. Silva, T. Fujita, M. Chen, T. Asefa, V. Shenoy, G. Eda and M. Chhowalla, "Conducting MoS₂ nanosheets as catalysts for hydrogen evolution reaction," *Nano Letters*, vol. 13, no. 12, pp. 6222-6227, 2013.

- [12] D. Voiry, H. Yamaguchi, J. Li, R. Silva, D. Alves, T. Fujita, M. Chen, T. Asefa, V. Shenoy and G. Eda, "Enhanced catalytic activity in strained chemically exfoliated WS₂ nanosheets for hydrogen evolution," *Nature Materials*, vol. 12, no. 9, pp. 850-855, 2013.
- [13] J. Yang and H. Shin, "Recent advances in layered transition metal dichalcogenides for hydrogen evolution reaction," *Journal of Materials Chemistry A*, vol. 2, no. 17, pp. 5979-5985, 2014.
- [14] E. P. Nguyen, T. Daeneke, S. Zhuiykov and K. Kalantar-zadeh, "Liquid Exfoliation of Layered Transition Metal Dichalcogenides for Biological Applications," *Current Protocols in Chemical Biology*, vol. 8, no. 2, pp. 97-108, 2016.
- [15] J. Liu, T. Lo, J. Sun, C. Yip, C. Lam and D. Lei, "A comprehensive comparison study on the vibrational and optical properties of CVD-grown and mechanically exfoliated few-layered WS₂," *Journal of Materials Chemistry C*, vol. 5, no. 43, pp. 11239-11245, 2017.
- [16] H. Lin, J. Wang, Q. Luo, H. Peng, C. Luo, R. Qi, R. Huang, J. Travas-Sejdic and C.-G. Duan, "Rapid and highly efficient chemical exfoliation of layered MoS₂ and WS₂," *Journal of Alloys and Compounds*, vol. 699, pp. 222-229, 2017.
- [17] H. Liu, L. Xu, W. Liu, B. Zhou, Y. Zhu, L. Zhu and X. Jiang, "Production of mono- to few-layer MoS₂ nanosheets in isopropanol by a salt-assisted direct liquid-phase exfoliation method," *Journal of Colloid and Interface Science*, vol. 515, pp. 27-31, 2018.
- [18] J. Dunklin, "Plasmon-mediated energy conversion in metal nanoparticle-doped hybrid nanomaterials," *University of Arkansas Theses and Dissertations*, p. 1986, 2017.
- [19] C. Backes, B. M. Szydłowska, A. Harvey, S. Yuan, V. Vega-Mayoral, B. R. Davies, P. L. Zhao, D. Hanlon, E. J. G. Santos and M. I. Katsnelson, "Production of highly monolayer enriched dispersions of liquid-exfoliated nanosheets by liquid cascade centrifugation," *ACS Nano*, vol. 10, no. 1, pp. 1589-1601, 2016.
- [20] L. Cheng, W. Huang, Q. Gong, C. Liu, Z. Liu, Y. Li and H. Dai, "Ultrathin WS₂ nanoflakes as a high-performance electrocatalyst for the hydrogen evolution reaction," *Angew. Chemie Int. Ed.*, vol. 53, no. 30, pp. 7860-7863, 2014.
- [21] D. Roper, J. Dunklin and A. O'Brien, "Enhanced Catalysis by Optical Nanoantenna Reduced on Transition Metal Dichalcogenide," in *Nano-Micro Conference*, Shanghai, 2017.
- [22] Z. Gholamvand, D. McAteer, C. Backes, N. McEvoy, A. Harvey, N. Berner, D. Hanlon, C. Bradley, I. Godwin, A. Rovetta, M. Lyons, G. Duesberg and J. Coleman, "Comparison of liquid exfoliated transition metal dichalcogenides reveals MoSe₂ to be the most effective hydrogen evolution catalyst," *Nanoscale*, vol. 8, no. 10, pp. 5737-5749, 2016.

- [23] Z. Seh, J. Kibsgaard, C. Dickens, I. Chorkendorff, J. Norskov and T. Jaramillo, "Combining theory and experiment in electrocatalysis: Insights into materials design," *Science*, vol. 355, no. 6321, 2017.
- [24] L. Ma, L. Ting, V. Molinari, C. Giordano and B. S. Yeo, "Efficient hydrogen evolution reaction catalyzed by molybdenum carbide and molybdenum nitride nanocatalysts synthesized via the urea glass route," *Journal of Materials Chemistry A*, vol. 3, no. 16, pp. 8361-8368, 2015.
- [25] X. Shang, K. L. Yan, Z. Z. Liu, S. S. Lu, B. Dong, J. Q. Chi, X. Li, Y. R. Liu, Y. M. Chai and C. G. Liu, "Oxidized carbon fiber supported vertical WS₂ nanosheets arrays as efficient 3D nanostructure electrocatalysts for hydrogen evolution reaction," *Appl. Surf. Sci.*, vol. 402, no. 120-128, 2017.
- [26] X. Guo, J. Ji, Q. Jiang, L. Zhang, Z. Ao, X. Fan, S. Wang, Y. Li, F. Zhang and G. Zhang, "Few-layered trigonal WS₂ nanosheet-coated graphite foam as an efficient free-standing electrode for a hydrogen evolution reaction," *ACS Appl Mater. Interfaces*, vol. 9, no. 36, pp. 30591-30598, 2017.
- [27] X. Huang, Z. Zeng, S. Bao, M. Wang, X. Qi, Z. Fan and H. Zhang, "Solution-phase epitaxial growth of noble metal nanostructures on dispersible single-layer molybdenum disulfide nanosheets," *Nature Communications*, vol. 4, pp. 1444-1448, 2013.
- [28] D. Merki, H. Vrubel, L. Rovelli, S. Fierro and X. Hu, "Fe, Co, and Ni ions promote the catalytic activity of amorphous molybdenum sulfide films for hydrogen evolution," *Chem Sci*, vol. 3, no. 8, pp. 2515-2525, 2012.
- [29] X. Lv, G. W. She, S. X. Zhou and Y. M. Li, "Highly efficient electrocatalytic hydrogen production by nickel promoted molybdenum sulfide microspheres catalysts," *RSC Adv.*, vol. 3, no. 44, pp. 21231-21236, 2013.
- [30] J. R. Dunklin, P. Lafargue, T. M. Higgins, G. T. Forcherio, M. Benamara, N. McEvoy, D. K. Roper, J. N. Coleman, Y. Vaynzof and C. Backes, "Monolayer-enriched production of Au-decorated WS₂ nanosheets via defect engineering," *MRS Adv.*, vol. 3, no. 41, pp. 2435-2440, 2018.
- [31] Y. Zhang, J. Yan, X. Ren, L. Pang, H. Chen and S. Liu, "2D WS₂ nanosheet supported Pt nanoparticles for enhanced hydrogen evolution reaction," *Int. J. Hydrogen Energy*, vol. 42, no. 8, pp. 5472-5477, 2017.
- [32] A. O'Brien, R. Romo, C. Hackett, A. Lovelady, M. Benamara and V. Bejugam, "Platinum nanoparticle reduction enhances hydrogen evolution by WS₂ nanosheet," *Manuscript in preparation*.

- [33] J. Dunklin, P. Lafargue, T. F. G. Higgins, M. Benamara, N. McEvoy, D. K. Roper, J. Coleman, Y. Vaynzof and C. Backes, "Production of monolayer-rich gold-decorated 2H-WS₂ nanosheets by defect engineering," *npj 2D Materials and Applications*, vol. 1, no. 43, 2018.
- [34] G. Eda, H. Yamaguchi, D. Voiry, T. Fujita, M. Chen and M. Chhowalla, "Photoluminescence of chemically exfoliated MoS₂," *Nano Letters*, vol. 11, no. 12, pp. 5111-5116, 2011.
- [35] Y. Qian, C. Wang and Z. Le, "Decorating graphene sheets with Pt nanoparticles using sodium citrate as reductant," *Appl. Surf. Sci.*, vol. 257, no. 24, pp. 10758-10762, 2011.
- [36] Z. Lv, X. Yang and E. Wang, "Highly concentrated polycations-functionalized graphene nanosheets with excellent solubility and stability, and its fast, facile and controllable assembly of multiple nanoparticles," *Nanoscale*, vol. 5, pp. 663-670, 2013.
- [37] Z. Fang, Y. Wang, J. Song, Y. Sun, J. Zhou, R. Xu and H. Duan, "Immobilizing CdS quantum dots and dendritic Pt nanocrystals on thiolated graphene nanosheets toward highly efficient photocatalytic H₂ evolution," *Nanoscale*, vol. 5, pp. 9830-9838, 2013.
- [38] L. A. Porter, H. C. Choi, A. E. Ribbe and J. M. Buriak, "Controlled electroless deposition of noble metal nanoparticle films on germanium surfaces," *Nano Letters*, vol. 2, no. 10, pp. 1067-1071, 2002.
- [39] T. Osaka, T. Misato, J. Sato, H. Akiya, T. Homma, M. Kato, Y. Okinaka and O. Yoshioka, "Evaluation of substrate (Ni)-catalyzed electroless gold plating process," *J. Electrochem. Soc.*, vol. 147, no. 3, pp. 1059-1064, 2000.
- [40] J. Byeon and J. Roberts, "Silver Deposition on a Polymer Substrate Catalyzed by Singly Charged Monodisperse Copper Nanoparticles," *ACS Appl. Mater. Interfaces*, vol. 4, pp. 2515-2520, 2012.
- [41] I. Capek, "Precursors and Their Conjugates," in *Noble Metal Nanoparticles: Preparation, Composite Nanostructures, Biodecoration, and Collective Properties*, Tokyo, Springer Japan, 2017, pp. 136-171.
- [42] X. Li, L. Zhang, X. Zang, X. Li and H. Zhu, "Photo-promoted platinum nanoparticles decorated MoS₂@graphene woven fabric catalyst for efficient hydrogen generation," *ACS Appl. Mater. Interfaces*, vol. 8, no. 17, pp. 10866-10873, 2016.
- [43] T. L. Tan, L. L. Wang, J. Zhang, D. D. Johnson and K. Bai, "Platinum nanoparticle during electrochemical hydrogen evolution: Adsorbate distribution, active reaction species, and size effect," *ACS Catal.*, vol. 5, no. 4, pp. 2376-2383, 2015.
- [44] Z. Gholamvand, "Comparison of liquid exfoliated transition metal dichalcogenides reveals MoSe₂ to be the most effective hydrogen evolution catalyst," *Royal Society of Chemistry*, vol. 8, no. 10, pp. 5737-5749, 2016.

- [45] T. Shinagawa, A. T. Garcia-Esparza and K. Takahabe, "Insight on Tafel slopes from a microkinetic analysis of aqueous electrocatalysis for energy conversion," *Sci. Rep.*, vol. 5, pp. 1-21, 2015.
- [46] S. Bai, C. Wang, M. Deng, M. Gong, Y. Bai, J. Jiang and Y. Xiong, "Surface polarization matters: Enhancing the hydrogen-evolution reaction by shrinking Pt shells in Pt-Pd-Graphene stack structures," *Angew. Chemie - Int Ed.*, vol. 53, no. 45, pp. 12120-12124, 2014.